Nonsequential two-photon absorption from the K shell in solid zirconium

Shambhu Ghimire,[1,*] Matthias Fuchs,[2] Jerry Hastings,[3] Sven C. Herrmann,[4] Yuichi Inubushi,[5] Jack Pines,[4] Sharon Shwartz,[6] Makina Yabashi,[5] and David A. Reis[1,7,†]

[1]*Stanford PULSE Institute, SLAC National Accelerator Laboratory, Menlo Park, California 94025, USA*
[2]*Department of Physics and Astronomy, University of Nebraska – Lincoln, Lincoln, Nebraska 68588, USA*
[3]*The Linac Coherent Light Source, SLAC National Accelerator Laboratory, Menlo Park, California 94025, USA*
[4]*SLAC National Accelerator Laboratory, Menlo Park, California 94025, USA*
[5]*RIKEN SPring-8 Center, Kouto 1-1-1 Sayo, Hyogo 679-5148, Japan*
[6]*Department of Physics, Institute for Nanotechnology and Advanced Materials, Bar Ilan University, Ramat Gan 52900, Israel*
[7]*Departments of Photon Science and Applied Physics, Stanford University, Stanford, California 94305, USA*

(Received 27 July 2016; published 21 October 2016)

We report the observation of nonsequential two-photon absorption from the K shell of solid Zr (atomic number $Z = 40$) using intense x-ray pulses from the Spring-8 Angstrom Compact Free-Electron Laser (SACLA). We determine the generalized nonlinear two-photon absorption cross section at the two-photon threshold in the range of 3.9–57 $\times 10^{-60}$ cm^4 s bounded by the estimated uncertainty in the absolute intensity. The lower limit is consistent with the prediction of 3.1 $\times 10^{-60}$ cm^4 s from the nonresonant Z^{-6} scaling for hydrogenic ions in the nonrelativistic, dipole limit.

DOI: 10.1103/PhysRevA.94.043418

I. INTRODUCTION

A wide array of multiphoton, nonlinear optical phenomena became accessible following the invention of the optical laser [1]. This includes the observation of two-photon absorption [2] and second-harmonic generation [3]. For hydrogenic ions the generalized cross section for an n-photon process (in the applied field) is expected to scale as Z^{-4n+2} in the dipole approximation at scaled frequency ωZ^{-2}, where Z is the nuclear charge, i.e., $\sigma^{(n)}(Z;\omega) = Z^{-4n+2}\sigma^{(n)}(1;\omega Z^{-2})$ [4]. Thus multiphoton interactions scale with the frequency as ω^{-2n+1}, and only with the advent of x-ray free-electron lasers (XFEL) [5,6] have nonsequential two-photon interactions become possible at hard x-ray energies. This includes two-photon Compton scattering by Fuchs *et al.* [7], x-ray second-harmonic generation by Shwartz *et al.* [8], and two-photon absorption by Tamasaku *et al.* [9].

Two-photon absorption (TPA) was first considered theoretically by Göppert-Mayer [10]. The general multiphoton absorption from the K shell of hydrogenic ions was considered by Lambropoulos and Tang [11]. Two-photon soft-x-ray absorption was measured by Doumy *et al.* [12] in heliumlike Ne at 1.110 keV, below the single-photon threshold (1.196 keV) but well above the two-photon threshold of half this value. The results were found to be 2–3 orders of magnitude higher than both the nonresonant perturbative scaling of Ref. [11] and the second-order perturbation theory calculations of Novikov and Hopersky [13], and were attributed to contributions from near-resonant states [14].

Recently Tamasaku *et al.* [9], measured two-photon absorption at 5.6 keV from the K shell of Ge ($Z = 32$) using intense x-ray pulses $\sim 10^{20}$ W/cm^2 at the nanometer-scale focal spot of the Spring-8 Angstrom Compact Free-Electron Laser (SACLA) [15]. The photon energy was just above half the single-photon threshold of 11.1 keV, and the results were consistent with nonresonant hydrogeniclike Z scaling. The measurement of the two-photon K-shell absorption cross section in elements with different nuclear charge is an important test of theory [4,16], including relativistic and retardation effects which can become important in the limit of high Z [17]. The measurements will impact future applications of ultrafast pulse metrology and nonlinear spectroscopy at x-ray wavelengths. Here we present the observation of below-threshold nonsequential two-photon absorption from the K shell of Zr ($Z = 40$). The experiments are carried out at the nanometer-scale focal spot of SACLA using a maximum peak intensity $\sim 3.6 \times 10^{18}$ W/cm^2 at photon energies near 9 keV (1.37 Å), half the Zr K edge (18 keV). We measure the generalized cross section at the two-photon threshold in the range of 3.9–57 $\times 10^{-60}$ cm^4 s bounded by systematic uncertainties in the absolute x-ray pulse intensity. This compares with the value of 3.1 $\times 10^{-60}$ cm^4 s from Z scaling.

II. EXPERIMENTS

The experiment is shown schematically in Fig 1. In Fig. 1(a) we show the process of TPA in Zr. The simultaneous interaction of two photons can lead to K-shell absorption only if the sum of their energies is greater than the threshold energy for single-photon absorption (18 keV for ground-state Zr). It creates a hole in the $1s$ shell that is filled primarily by K-fluorescence emission near 16 keV ($2p$-$1s$) in a 4π solid angle. The linearly polarized x-ray beam with a photon energy tunable near $\sim$9 keV with pulse duration $\leqslant$10 fs [6] was focused using two-stage reflective Kirkpatrick-Baez mirrors on a 25-μm thin Zr foil (positioned at an incidence angle of 45°) [Fig. 1(b)]. The focal spot was characterized using a knife-edge scan method. The average of several measurements yielded a focal area of 81×95 nm^2 FWHM containing $\sim$29% of the beam energy. The average pulse energy during the experiment after considering the loss from optics and without attenuators is 9.7$\pm$ 2.5 μJ. Therefore we expect

*shambhu@slac.stanford.edu
†dreis@slac.stanford.edu

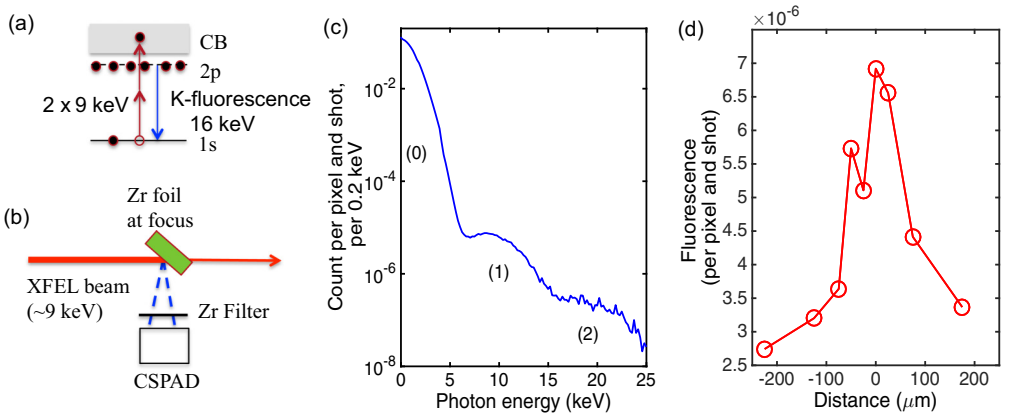

FIG. 1. (a) Schematic for nonsequential two-photon K-shell absorption in metallic Zr. When the incident photon energy exceeds half the single-photon K-absorption threshold (∼18 keV), a $1s$ vacancy can be created through the simultaneous absorption of two (or more) photons. This vacancy is primarily filled by radiative decay from the $2p$ state in the form of K_α fluorescence. (b) A powerful XFEL beam near 9 keV is focused to a submicron spot on a 25-μm thin Zr foil. The fluorescent signal is collected at 90 deg in the polarization plane using a 140-K pixel single-photon-sensitive detector. A 50-μm Zr filter is inserted in front of the detector to reduce the background from scattered photons. (c) A representative detector histogram accumulated over 3000 shots, where peaks (0), (1), and (2) correspond to pixels registering zero photons, single photons near the fundamental (∼9 keV), and single photons near the K-fluorescence peak (∼16 keV), respectively, for an incident pulse energy of ∼10 μJ. The background from the pileup from two 9-keV photons in a single pixel has been suppressed as described in the text. (d) Dependence of peak (2) as the sample is scanned through the focal plane.

up to $\sim 2 \times 10^9$ photons in the focus. In order to suppress the background from linear single-photon K-shell ionization, the FEL harmonic content on the target was substantially suppressed by the four reflections from the mirrors, which have a high-energy cutoff of 15 keV. A portion of the K fluorescence was collected near 90° in the polarization plane, where the scattering from the polarized beam is expected to be minimum. A Cornell-SLAC hybrid pixel array detector (CSPAD) 140-K pixel array detector with 110×110 μm^2 pixels [18] was positioned at 33 cm from the target such that each pixel subtends $\Delta\Omega = 1.1 \times 10^{-7}$ srad, corresponding to a total solid angle of $\sim 15 \times 10^{-3}$ srad. To further suppress the background due to scattering, a Zr filter was inserted in front of the CSPAD. For a 50-μm filter this decreases the background near the FEL fundamental by about 2 orders of magnitude while allowing about 50% percent transmission at ∼16 keV. At the intensities used here, the FEL damages the sample on a single shot, and therefore we translated the sample to an undamaged region between shots at the beam repetition rate of 10 Hz.

A representative detector histogram averaged over 3000 shots and normalized by the number of pixels is shown in Fig. 1(c) at an incident energy of 9.10 keV with a bandwidth of ∼0.050 keV [6], and at the highest intensity used, $\sim 3 \times 10^{18}$ W/cm^2. The data are binned according to x-ray photon energy converted from the charge collected assuming a single photon is absorbed in a pixel. Individual detector frames were corrected for gain nonuniformity and a common-mode offset [18]. By far the dominant peak (0) corresponds to pixels in which no photons were absorbed, and the width corresponds to the electronic noise under dark conditions.

The peaks (1) and (2) correspond to the residual scattered x rays near the FEL fundamental and higher-energy photons, including the $K_{\alpha,\beta}$ fluorescence signals (15.6 keV and 17.6 keV), respectively. The higher-energy peak (2) has also been corrected on each shot to remove the pileup from two or more fundamental photons. Under uniform illumination of the detector, the probability of measuring two photons in a single pixel in a single shot is negligible ($<10^{-10}$). However, elastic scattering from a single grain of our polycrystalline sample leads to a nonuniform illumination that was removed in postprocessing by identifying clusters of photons.

In Fig. 1(d) we plot the integrated counts of peak (2) as a function of the distance of the sample from the location of the nominal beam waist (at a fixed pulse energy). This shows a clear dependence on the sample position and thus beam area. If peak 2 were from pileup, the counts would decrease as we scan the sample through the focus, since a smaller number of grains are illuminated with a decreased interaction area. The observed rapid increase is consistent with a perturbative nonlinear two-photon absorption process that scales inversely with the area. The width of the peak is reasonably consistent with an estimate for the depth of focus based on a lowest order Gaussian beam and nonastigmatic focusing. Here $2z_R = 2\pi w^2/\lambda = 260$ μm, where $w = 2\sigma$ is the waist diameter (average of 75 nm) and λ is the wavelength (1.36 Å at 9.1 keV).

The intensity dependence of the integrated higher-energy peak (2) for both above (9.1 keV) and below (8.9 keV) the two-photon threshold is shown in Fig. 2. The fundamental is attenuated by inserting Al and/or Si filters upstream of the focusing optics. Due to their strong chromaticity, the transmission for the FEL harmonics is relatively unaffected. (Note that at the maximum attenuation used here, the transmission of the fundamental is ∼4%, while it is ∼66% and ∼88% for the second and third harmonic, respectively.) Thus any linear ionization due to residual harmonic contamination would produce a nearly constant background, which corresponds to <5% of the signal at the highest intensity. Above the two-photon threshold, the data show a clear quadratic dependence consistent with the TPA process. Below the two-photon

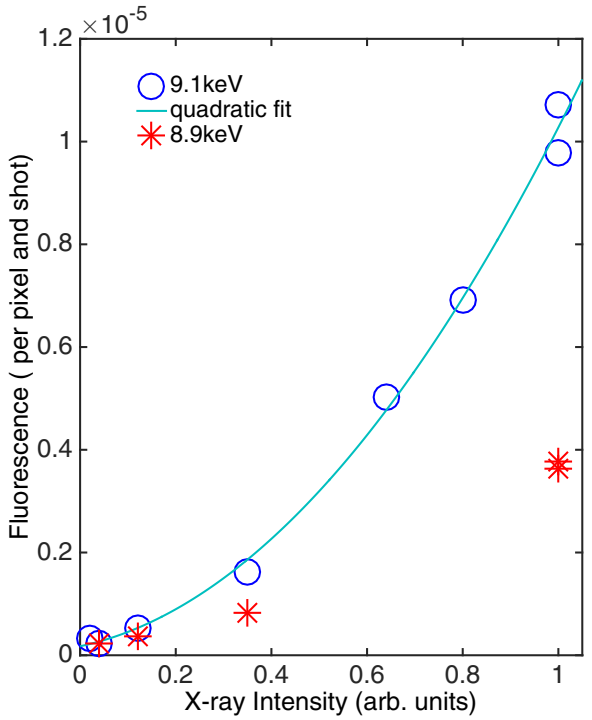

FIG. 2. X-ray intensity dependence of the K fluorescence when incident photon energy is above (9.1 keV) and below (8.9 keV) the TPA threshold. Above-threshold data is represented by circles. Below-threshold data is represented by asterisks. This data is obtained by integrating peak (2) of the histogram as shown in Fig. 1(c). Above-threshold data depends quadratically on the intensity (solid line). Below-threshold measurements show a weaker nonlinearity compared to above threshold. Measurements were averaged over 3000 shots, and the statistical error due to photon counting is smaller than the size of the symbol.

threshold, peak (2) is weaker and is $\sim 1/3$ of the signal above threshold. The presence of nonlinear background could be due to two-photon Compton scattering (TPC), such as seen recently in Be by Fuchs *et al.* [7]. In the case of Zr, this would correspond the simultaneous scattering of two photons from an electron outside the K shell producing a single photon redshifted from twice the photon energy. One way to distinguish the relative contributions of TPA and TPC is by the behavior near half the K edge; only the former should show a threshold behavior in the high-energy peak. Figure 3(a) shows histograms for incident photon energies around the TPA threshold energies taken in 0.05-keV steps (corresponding to the approximate FEL bandwidth) at the highest intensity, while Fig. 3(b) shows the integrated higher-energy peak. In this case, we use a 100-μm Zr filter in front of the detector. This accounts for only about a factor of 2 of the decrease in count rate compared to Fig. 2. There is a step in the higher-energy peak (2) at 9.00 keV consistent with the TPA threshold. Below this threshold the peak is lowered by about a factor of 3, consistent with Fig. 2; thus we conclude that the lower count rate is likely due to the sample drifting out of the focal plane. We further conclude that approximately 2/3 of the counts above threshold are due to the TPA signal. Note that we do not expect to resolve two-photon resonances below the edge because of the large FEL bandwidth (50 eV), which is about an order of magnitude larger than the width of the $1s$ state.

III. ABSORPTION CROSS SECTION

We extract the two-photon cross section from the measurement as follows. The rate of producing a K-shell vacancy by two-photon absorption of any given Zr atom $\Gamma^{(2)} = \sigma_\omega^{(2)} F_\omega^2$ [19], where F_ω is the photon flux at the fundamental frequency ω. Assuming a Gaussian beam in time and space and in the limit of an optically thick sample for the fundamental, the number of $1s$ vacancies produced in a single pulse is

$$N_{1s} = \sqrt{\frac{\ln(2)}{8\pi}} \frac{N_\omega^2 \sigma_\omega^{(2)}}{A \Delta\tau \sigma_\omega^{(1)}}, \tag{1}$$

where N_ω is the number of photons, $A = \frac{\pi}{2} w_x w_y$ is the beam area, and $\Delta\tau$ is the pulse duration (FWHM). $\sigma_\omega^{(1)}$ is the linear attenuation cross section, which is dominated by L-shell photoionization since we are below the single-photon K-shell threshold (1.46×10^{-20} cm^2 at 9 keV). Thus, from the measured number of fluorescent photons per pixel N_K,

$$\sigma_\omega^{(2)} = \sqrt{\frac{8\pi}{\ln(2)}} \frac{4\pi N_K}{\Delta\Omega Y \epsilon} \frac{A\Delta\tau}{N_\omega^2} \sigma_\omega^{(1)}, \tag{2}$$

where $Y = 0.74$ is the florescent yield [20] and $\epsilon = 0.32$ is the detection efficiency, including the quantum efficiency of the detector and Zr filter transmission.

We use the data from Fig. 2, where at the highest intensity, the measured fluorescence rate is 6×10^{-6}/pixel/shot, after subtracting the background counts at 8.9 keV. Thus we extract an upper limit of $\sigma_\omega^{(2)} = 57 \times 10^{-60}$ cm^4 s. Both a shorter pulse duration or the expected spiky nature due to the Self-amplified Spontaneous Emission (SASE) process would result in a lower measured cross section. If we use 2.5 fs for the pulse duration as used in Ref. [9], the extracted cross section would be reduced by a factor of 4. Similarly, a higher fraction of the beam in the focal spot would result in lower measured cross section. As it was done in Tamasaku *et al.* [9], if we assume that 55% of the beam is in the focal spot, then the measured cross section would be lower by another factor of 3.6. This results in a lower estimate of the cross section of 3.9×10^{-60} cm^4 s.

In Fig. 4 we compare our measured TPA cross section from the K shell of Zr with the theoretical Z^{-6} scaled results from the hydrogen atom at threshold and other experimental results at different Z. The calculation results on H were taken from [21,22]. The experimental data for He, He-like Ne, and Ge are taken from Ref. [23], Ref. [12], and Ref. [9], respectively. We note that He experiments were performed above the one-photon threshold where it competes with two-photon double ionization. The He-like Ne results were also measured far from the two-photon threshold, and the relative difference from perturbative scaling was attributed to the contributions from near-resonant states [14]. In the current work on Zr, the upper (lower) limit of the cross section is about 23 (1.3) times higher than the Z^{-6} scaled results for $Z = 40$.

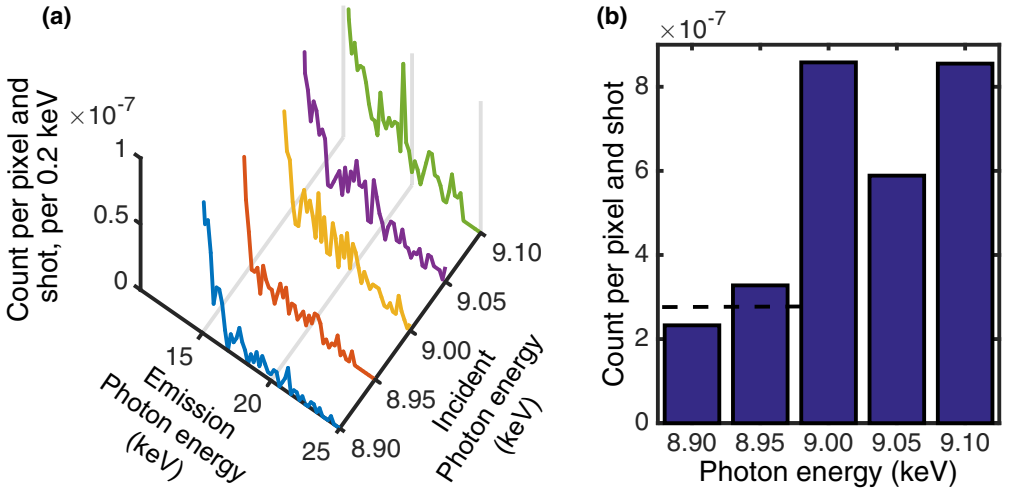

FIG. 3. Photon energy threshold for two-photon absorption in Zr K shell. In (a) a section of histograms are shown for x-ray photon energy just below and just above the TPA threshold of 9 keV. Histograms were averaged over 3000 shots. The higher-energy peak (counts >15.5 keV) is seen at and above the threshold. A 100-μm Zr filter was used in this measurement. (b) The integrated count within the high-energy peak as a function of photon energy. The photon energy is changed in 50-eV steps. The total count at 9 keV is about 3 times higher than the noise level, shown by the dashed line below the threshold.

IV. DISCUSSION AND OUTLOOK

In conclusion, nonsequential two-photon absorption in the K shell of solid Zr was observed at a peak intensity of $\sim 10^{18}$ W/cm^2 using the nanofocus x-ray beam at the Spring-8 Angstrom Compact Free-Electron Laser. The two-photon absorption process was verified from the nonlinear intensity dependence of the K-fluorescence signal and a careful characterization of the background from the elastic scattering, linear photoionization from the FEL harmonics. Below threshold we measure a nonlinear contribution to the signal that is possibly due to nonresonant two-photon Compton scattering. More detailed measurements of the angular distribution and spectrum would allow us to further separate the TPA and TPC processes, as the former produces K florescence, which is narrow and emitted into 4π, and the latter a broad spectrum emitted in a nondipolar angular distribution [7].

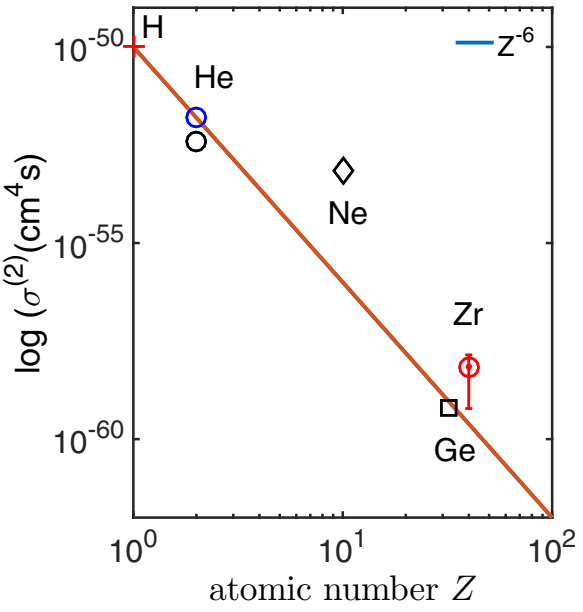

FIG. 4. Comparison of K-shell TPA cross section from solid Zr to the Zernik Z^{-6} scaling along with experimental results in other elements with different Z. The solid line represents the Zernik scaling for the nonresonant, nonrelativistic, and dipole limit at threshold for the H-like ions, referencing to the calculated cross section in H atom 1.27×10^{-50} cm^4 s [21,22]. The data for He is for 41.8 eV, above the single-photon threshold, taken from [23]. The value for Ne^{8+} is taken from Ref. [12]. The measurement for Ge is taken from Ref. [9].

From a comparison of the nonlinear signal above and below threshold we extract the generalized two-photon absorption cross section in the range of 3.9–57 $\times 10^{-60}$ cm^4 s bounded by the estimated systematic uncertainty in the beam parameters that determine the absolute intensity. This compares to the prediction 3.1×10^{-60} cm^4 s from the nonresonant Z^{-6} scaling for hydrogenic ions in the nonrelativistic dipole limit. A more precise knowledge of the x-ray spatiotemporal profile and the use of fully coherent beams (seeded operation [24]) would be beneficial to further minimize the measurement errors for a detailed comparison with theory and also to resolve resonance effects. Alternatively, one could remove the need to rely on precise knowledge of the spot size by the use of sufficiently small nanoparticles combined with coherent imaging to extract the particle size and ratio of linear-to-nonlinear scattering. Uniform illumination can be ensured by injecting nanoparticles into the beam whose dimensions are sufficiently smaller than the x-ray focal volume and attenuation length. In this case the x-ray photon flux on the particle can be obtained from the diffraction image on a single-shot basis. This process requires knowledge of the particle shape and size. Both size and shape can in principle be obtained from the inversion of the diffraction image using single-particle coherent x-ray diffraction imaging techniques [25,26], while the photon number is extracted from the integrated intensity of the diffraction pattern. This leaves the temporal pulse shape as the largest uncertainty. Such a method would be insensitive

to particle placement in the focus, as both the illumination and the particle size are obtained on each shot, allowing for postsorting the data. We note that the two-photon absorption process itself has a potential for future x-ray temporal pulse metrology. The development of a robust x-ray pulse width and intensity measurement is critical for better understanding of nonlinear x-ray matter interactions at free-electron lasers. Here a nonlinear signal such as in two-photon absorption could be used to perform intensity autocorrelations of the pulse duration, which may be extendable to a single-shot measurement that could resolve the chaotic structure in the SASE pulse. Finally, we note that two-photon absorption spectroscopy could prove useful as an instantaneous probe of excited-state dynamics with chemical specificity, as well as provide better sensitivity for K-shell spectroscopy to connect to d-like states due to the different angular momentum dipole selection rules for nonlinear absorption.

Note added in proof. Szlachetcko *et al*. recently reported two-photon x-ray absorption in Cu just below the one-photon K-shell ionization threshold [27].

ACKNOWLEDGMENTS

This research was primarily supported by the AMOS program within the Chemical Sciences Division of the Office of Basic Energy Sciences, Office of Science, U.S. Department of Energy. M.F. acknowledges support by the Volkswagen Foundation. The XFEL experiments were performed at the BL3 of SACLA with the approval of the Japan Synchrotron Radiation Research Institute (JASRI) (Proposal No. 2012B8004). We thank the LCLS detector team for providing the CSPAD detector and Philip Hart for advice on the analysis.

[1] T. Maiman, Stimulated optical radiation in ruby, Nature (London) **187**, 493 (1960).

[2] W. Kaiser and C. G. B. Garrett, Two-Photon Excitation in CaF_2: Eu^{2+}, Phys. Rev. Lett. **7**, 229 (1961).

[3] P. A. Franken, A. E. Hill, C. W. Peters, and G. Weinreich, Generation of Optical Harmonics, Phys. Rev. Lett. **7**, 118 (1961).

[4] L. B. Madsen and P. Lambropoulos, Scaling of hydrogenic atoms and ions interacting with laser fields: Positronium in a laser field, Phys. Rev. A **59**, 4574 (1999).

[5] P. Emma, First lasing and operation of an ångstrom-wavelength free-electron laser, Nat. Photonics **4**, 641 (2010).

[6] T. Ishikawa, H. Aoyagi, T. Asaka, Y. Asano, N. Azumi, T. Bizen, H. Ego, K. Fukami, T. Fukui, Y. Furukawa, S. Goto, H. Hanaki, T. Hara, T. Hasegawa, T. Hatsui, A. Higashiya, T. Hirono, N. Hosoda, M. Ishii, T. Inagaki *et al.*, A compact X-ray free-electron laser emitting in the sub-ångstrom region, Nat. Photonics **6**, 540 (2012).

[7] M. Fuchs, M. Trigo, J. Chen, S. Ghimire, S. Shwartz, M. Kozina, M. Jiang, T. Henighan, C. Bray, G. Ndabashimiye, P. H. Bucksbaum, Y. Feng, S. Herrmann, G. A. Carini, J. Pines, P. Hart, C. Kenney, S. Guillet, S. Boutet, G. J. Williams, M. Messerschmidt, M. M. Seibert, S. Moeller, J. B. Hastings, and D. A. Reis, Anomalous nonlinear x-ray compton scattering, Nat. Phys. **11**, 964 (2015).

[8] S. Shwartz, M. Fuchs, J. B. Hastings, Y. Inubushi, T. Ishikawa, T. Katayama, D. A. Reis, T. Sato, K. Tono, M. Yabashi, S. Yudovich, and S. E. Harris, X-Ray Second Harmonic Generation, Phys. Rev. Lett. **112**, 163901 (2014).

[9] K. Tamasaku, E. Shigemasa, Y. Inubushi, T. Katayama, K. Sawada, H. Yumoto, H. Ohashi, H. Mimura, M. Yabashi, K. Yamauchi, and T. Ishikawa, X-ray two-photon absorption competing against single and sequential multiphoton processes, Nat. Photonics **8**, 313 (2014).

[10] M. Göppert-Mayer, Über Elementarakte mit zwei Quantensprüngen, Ann. Phys. (Berlin, Ger.) **401**, 273 (1931).

[11] P. Lambropoulos and X. Tang, Multiple excitation and ionization of atoms by strong lasers, J. Opt. Soc. Am. B **4**, 821 (1987).

[12] G. Doumy, C. Roedig, S.-K. Son, C. I. Blaga, A. D. DiChiara, R. Santra, N. Berrah, C. Bostedt, J. D. Bozek, P. H. Bucksbaum, J. P. Cryan, L. Fang, S. Ghimire, J. M. Glownia, M. Hoener, E. P. Kanter, B. Krässig, M. Kuebel, M. Messerschmidt, G. G. Paulus, D. A. Reis, N. Rohringer, L. Young, P. Agostini, and L. F. DiMauro, Nonlinear Atomic Response to Intense Ultrashort X Rays, Phys. Rev. Lett. **106**, 083002 (2011).

[13] S. A. Novikov and A. N. Hopersky, Two-photonexcitation-ionization of the 1s shell of highly charged positive atomic ions, J. Phys. B: At., Mol. Opt. Phys. **34**, 4857 (2001).

[14] A. Sytcheva, S. Pabst, S.-K. Son, and R. Santra, Enhanced nonlinear response of Ne^{8+} to intense ultrafast x rays, Phys. Rev. A **85**, 023414 (2012).

[15] H. Mimura, H. Yumoto, S. Matsuyama, T. Koyama, K. Tono, Y. Inubushi, T. Togashi, T. Sato, J. Kim, R. Fukui *et al.*, Generation of 10^{20}Wcm^{-2} hard X-ray laser pulses with two-stage reflective focusing system, Nat. Commun. **5**, 3539 (2014).

[16] W. Zernik, Two-photon ionization of atomic hydrogen, Phys. Rev. **135**, A51 (1964).

[17] P. Koval, S. Fritzsche, and A. Surzhykov, Relativistic and retardation effects in the two-photon ionization of hydrogen-likeions, J. Phys. B: At., Mol. Opt. Phys. **36**, 873 (2003).

[18] S. Herrmann, S. Boutet, B. Duda, D. Fritz, G. Haller, P. Hart, R. Herbst, C. Kenney, H. Lemke, M. Messerschmidt, J. Pines, A. Robert, M. Sikorski, and G. Williams, CSPAD-140k: A versatile detector for LCLS experiments, Nucl. Instrum. Methods Phys. Res., Sect. A **718**, 550 (2013), Proceedings of the 12th Pisa Meeting on Advanced Detectors La Biodola, Isola d'Elba, Italy, May 20–26, 2012.

[19] P. Lambropoulos, in *Advances in Atomic and Molecular Physics*, edited by D. R. Bates and B. Bederson (Academic Press, New York, 1976), Vol. 12, pp. 87–164.

[20] A. Thompson *et al.*, X-ray data booklet (2009), http://xdb.lbl.gov (2009).

[21] S. Klarsfeld, Two-photon ionization of atomic hydrogen in the ground state, Lett. Nuovo Cimento Soc. Ital. Fis. **3**, 395 (1970).

[22] E. Karule, On the evaluation of transition matrix elements for multiphoton processes in atomic hydrogen, J. Phys. B: At. Mol. Phys. **4**, L67 (1971).

[23] H. Hasegawa, E. J. Takahashi, Y. Nabekawa, K. L. Ishikawa, and K. Midorikawa, Multiphoton ionization of He by using intense high-order harmonics in the soft-x-ray region, Phys. Rev. A **71**, 023407 (2005).

[24] J. Amann, W. Berg, V. Blank, F.-J. Decker, D. Zhu *et al.*, Demonstration of self-seeding in a hard-X-ray free-electron laser, Nat. Photonics **6**, 693 (2012).

[25] N. Loh, C. Y. Hampton, A. V. Martin, D. Starodub, R. G. Sierra, A. Barty, A. Aquila, J. Schulz, L. Lomb, J. Steinbrener *et al.*, Fractal morphology, imaging and mass spectrometry of single aerosol particles in flight, Nature (London) **486**, 513 (2012).

[26] N. D. Loh, D. Starodub, L. Lomb, C. Y. Hampton, A. V. Martin, R. G. Sierra, A. Barty, A. Aquila, J. Schulz, J. Steinbrener, R. L. Shoeman, S. Kassemeyer, C. Bostedt, J. Bozek, S. W. Epp, B. Erk, R. Hartmann, D. Rolles, A. Rudenko, and B. Rudek, Sensing the wavefront of x-ray free-electron lasers using aerosol spheres, Opt. Express **21**, 12385 (2013).

[27] J. Szlachetko, J. Hoszowska, J.-C. Dousse, M. Nachtegaal, W. Błachucki, Y. Kayser, J. Sà, M. Messerschmidt, S. Boutet, G. J. Williams, C. David, G. Smolentsev, J. A. van Bokhoven, B. D. Patterson, T. J. Penfold, G. Knopp, M. Pajek, R. Abela, and C. J. Milne, Establishing nonlinearity thresholds with ultraintense X-ray pulses, Sci. Rep. **6**, 33292 (2016).